Dalton Transactions

COMMUNICATION

View Article Online
View Journal | View Issue

Cite this: *Dalton Trans.*, 2017, **46**, 14752

Received 31st August 2017,
Accepted 3rd October 2017

DOI: 10.1039/c7dt03223d

rsc.li/dalton

Enhanced thermoelectric performance in ternary spinel $Cu_4Mn_2Te_4$ *via* the synergistic effect of tellurium deficiency and chlorine doping†

Hong Chen,[a] Hua Lin, *[a] Yi Liu, [b] Xin-Tao Wu[a] and Li-Ming Wu *[a,c]

The chemistry of copper-based chalcogenides has received considerable attention due to their diverse structures and potential applications in the area of thermoelectric (TE) materials. In this communication, a series of spinel-type $Cu_4Mn_2Te_4$-based samples have been successfully prepared and their high TE performances are attributed to the enhanced power factor and low thermal conductivity *via* the synergistic effect of Te deficiency and Cl doping. Consequently, a maximum TE figure of merit (*ZT*) of ~0.4 was achieved for the $Cu_4Mn_2Te_{3.93}Cl_{0.03}$ sample at 700 K, which was about 100% enhanced in comparison with the undoped $Cu_4Mn_2Te_4$ sample and one of the highest *ZT* values reported for p-type spinel tellurides.

With the rapid growth of global energy consumption and the increasing depletion of fossil fuels, great attention has been paid to the environmentally friendly and reliable thermoelectric (TE) materials due to their capability of converting heat into electricity.[1–6] The energy conversion efficiency of a TE material is determined by the dimensionless figure of merit, $ZT = (S^2\sigma)T/\kappa = PFT/\kappa$, where S, σ, κ, T and PF are the Seebeck coefficient, electrical conductivity, total thermal conductivity, absolute temperature and power factor, respectively.[7] Among these, κ contains the lattice thermal conductivity (κ_l) and electronic thermal conductivity (κ_e). In general, outstanding TE performance in a material requires achieving simultaneously high S, large σ and low κ. However, this is an enormous challenge because these parameters (S, σ and κ) are interrelated to each other. Over the past few decades, significant efforts have been made to obtain a high *ZT* value *via* maximizing the *PF* (including band engineering, resonant states, modulation doping, energy barrier filtering, and so forth)[8–12] and/or minimizing κ (including point defect scattering, grain boundary scattering, interface scattering, nano-structuring, "rattling", *etc.*).[3,13–16] Recent advances show that TE systems with intrinsically low κ_l can achieve high *ZT* values. One of the most exciting findings in this field is solid-state copper-based chalcogenides, not only for their fascinating structural features but also for their high TE performances.[16–29] For instance, binary copper-deficient $Cu_{2-x}Q$ (Q = S, Se and Te) systems as typical "phonon-liquid electron-crystal" (PLEC) materials exhibit ultralow κ_l (0.3–0.6 W m^{-1} K^{-1}) and high *ZT* values (1.5–2.1) based on the highly disordered Cu ions at high temperatures.[20–26] Very low κ_l (<0.5 W m^{-1} K^{-1}) was observed in ternary $Cu_{12}Sb_4S_{13}$, which was attributed to its unique tetrahedrite crystal structure (including CuS_4, CuS_3 and SbS_3 building units).[27] $Ba_5Cu_8In_2S_{12}$, a quaternary semiconductor with a 3D copper-rich framework, shows exceptionally low κ_l (*ca.* 0.3 W m^{-1} K^{-1} at 773 K).[28]

With the above considerations in mind, we focused our interest on ternary $Cu_4Mn_2Te_4$ thanks to the disordering of Cu ions in the spinel structure, which may create its intrinsic high conductivity and low thermal conductivity characteristics. The crystal structure and magnetic properties of this compound were first investigated by Lotgering and co-workers in 1972.[30] Subsequently, the temperature dependence of σ and S of $Cu_{4-x}Mn_2Te_4$ (x = −0.1, 0, 0.5) in a wide range of temperatures (473–923 K) was studied by Valiev, L. M. *et al.*[31] And benefiting from the very large σ and moderate S, all of the samples have large *PF* ($PF = S^2\sigma$) at high temperatures (5.4×10^{-4}–2.4×10^{-3} μW cm^{-1} K^{-2}).[31] Moreover, as suggested by Spitzer, the spinel structure may favour low κ_l due to the strong phonon scattering.[32] However, to the best of our knowledge, their complete thermal transport properties have not been investigated.

In this communication, for the first time, we studied the complete TE performance of the Cu-based spinel-type $Cu_{4+x}MnTe_{4-\delta-y}Cl_y$ (x = 0/0.01/0.02, δ = 0, y = 0; x = 0, δ = 0.02/0.04, y = 0; x = 0, δ = 0.04, y = 0.02/0.03/0.04). The synergistic

[a]*State Key Laboratory of Structural Chemistry, Fujian Institute of Research on the Structure of Matter, Chinese Academy of Sciences, Fuzhou, Fujian 350002, People's Republic of China. E-mail: linhua@fjirsm.ac.cn, liming_wu@fjirsm.ac.cn*
[b]*State Key Laboratory of Silicon Materials, School of Materials Science and Engineering, Zhejiang University, Hangzhou 310027, People's Republic of China*
[c]*Beijing Key Laboratory of Energy Conversion and Storage Materials, College of Chemistry, Key Laboratory of Theoretical and Computational Photochemistry, Ministry of Education, Beijing Normal University, Beijing 100875, People's Republic of China*

†Electronic supplementary information (ESI) available: Experimental section, together with additional figures and tables. See DOI: 10.1039/c7dt03223d

effect of tellurium deficiency and chlorine doping effectively increased *PF* and decreased κ. Consequently, the ZT_{max} value of about 0.4 was achieved for the $Cu_4Mn_2Te_{3.93}Cl_{0.03}$ sample at 700 K, which was about 100% enhanced in comparison with the un-doped $Cu_4Mn_2Te_4$ sample.

Samples of $Cu_{4+x}MnTe_{4-\delta-y}Cl_y$ (x = 0/0.01/0.02, δ = 0, y = 0; x = 0, δ = 0.02/0.04, y = 0; x = 0, δ = 0.04, y = 0.02/0.03/0.04) were synthesized by a conventional high-temperature solid-state reaction with a stoichiometric element mixture. As shown in Fig. 1a, the phase purity of the as-synthesized samples was confirmed from the powder XRD data and no impure phase was observed within the detection limits of the equipment. As shown in Fig. S1a,† DTA performed on the as-synthesized $Cu_4Mn_2Te_4$ shows no obvious mass loss in the measured temperature range (300–1073 K). This was confirmed by the powder XRD patterns of the sample before and after hot pressing, as shown in Fig. S2.† In addition, the DSC curves show an endothermic peak (*ca.* 742 K) in the heating process and an exothermal peak (*ca.* 723 K) in the cooling process (as shown in Fig. S1b†), which associates with a clear first-order structural phase change. These values were in good agreement with the literature data.[30,31] It is noteworthy that a very narrow phase width was observed in the $Cu_4Mn_2Te_4$ sample. For example, when x > 0.02, Cu impurity appeared; when δ > 0.04, a small amount of Cu and MnTe impurity appeared.

The idealized $Cu_4Mn_2Te_4$ structure has cubic symmetry (space group $Fd\bar{3}m$, Person symbol *cF*72), as depicted in Fig. 1b. Its asymmetric unit is comprised of two crystallographically independent Cu atoms, one Mn atom, and one independent Te atom, which occupy Wyckoff sites 8*b* (fully occupied by Cu1), 48*f* (50% occupied by Cu2), 16*c* and 32*e*, respectively (Fig. 1, bottom).[30] The structure can be described as two interpenetrating networks. The $MnTe_6$ octahedra share edges to form a three-dimensional labyrinth of channels, within which 3D $Cu2Te_4$-based anionic frameworks exist. The two networks are linked through the interaction between the dispersed $Cu1Te_4$ tetrahedron and the shared vertex framework tellurides.

Fig. 2 shows the temperature dependence of the electrical transport properties [electrical conductivity (σ) and Seebeck coefficient (S)] of the pristine $Cu_4Mn_2Te_4$ sample. An abnormal phase-transition around 730 K is observed both in the $\sigma(T)$ and $S(T)$ curves, which is confirmed by the DSC analysis (Fig. S1b, in the ESI†). Combining σ and S, we get a moderate

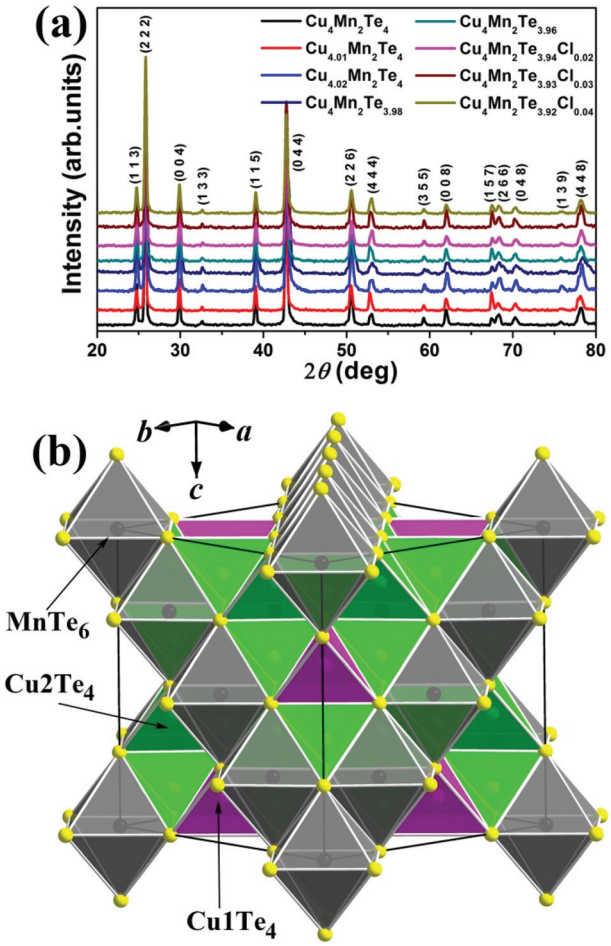

Fig. 1 (a) Powder XRD patterns of the as-synthesized polycrystalline $Cu_{4+x}Mn_2Te_{4-\delta-y}Cl_y$ samples at room-temperature with diffraction peaks indexed (x = 0/0.01/0.02, δ = 0, y = 0; x = 0, δ = 0.02/0.04, y = 0; x = 0, δ = 0.04, y = 0.02/0.03/0.04). (b) Crystal packing structure of $Cu_4Mn_2Te_4$ (space group $Fd\bar{3}m$) with the unit cell marked. Colour legends: Gray octahedron, $MnTe_6$; pink tetrahedron, $Cu1Te_4$; blue tetrahedron, $Cu2Te_4$.

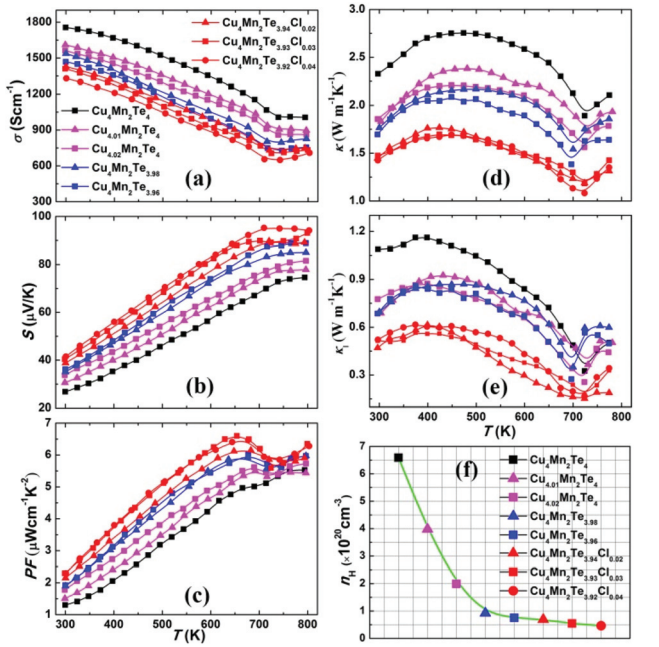

Fig. 2 Temperature dependence of (a) electrical conductivity (σ), (b) Seebeck coefficient (S), (c) power factor ($PF = S^2\sigma$), (d) total thermal conductivity (κ), (e) lattice thermal conductivity (κ_l) and (f) carrier concentration (n_H) at room temperature for polycrystalline $Cu_{4+x}Mn_2Te_{4-\delta-y}Cl_y$ samples (x = 0/0.01/0.02, δ = 0, y = 0; x = 0, δ = 0.02/0.04, y = 0; x = 0, δ = 0.04, y = 0.02/0.03/0.04). The Lorenz number (L) and electronic thermal conductivity (κ_e) are shown in Fig. S4.†

power factor *PF* (*ca.* 5 μW cm^{-1} K^{-2} at 700 K), which is lower than that of the un-doped $Cu_4Mn_2Te_4$ sample reported in the literature at the same temperature (*ca.* 20 μW cm^{-1} K^{-2}),[31] as indicated in Fig. S3.† Although we have attempted to adjust the synthesis processes to acquire the magnitude close to that in the literature,[31] we were not successful, and the TE transport properties do not exceed the data shown in Fig. 2.

Because of its extremely high electrical conductivity, the thermal conductivity of pristine $Cu_4Mn_2Te_4$ is also quite high, and the best *ZT* value is only approximately 0.2 at 720 K, which is not promising to ensure it as a decent TE material. As suggested by Hall measurement, pristine $Cu_4Mn_2Te_4$ exhibits the p-type conduction, and the room temperature carrier concentration (n_H) is more than 6.6 × 10^{20} cm^{-3}. This suggests that n_H must be substantially reduced to achieve a high *ZT* value.

On the one hand, we introduced Cu excess (noted **M1**) and Te vacancies (noted **M2**) as p-type doping, and brought down n_H to about 2.0 × 10^{20} cm^{-3} and 7.5 × 10^{19} cm^{-3} in $Cu_{4.02}Mn_2Te_4$ and $Cu_4Mn_2Te_{3.98}$, respectively. Accordingly, σ decreased and *S* increased from 300 K to 700 K when *x* (or δ) varied; the details of the change trend for all investigated samples are summarized in Table 1. It was very interesting to see that the electrical transport properties of different samples tended to converge as the temperature surpassed the phase-transformation temperature (>730 K), resulting in approximately the same *PF* at high temperatures. Consequently, *PF* increased by about 9% for $Cu_{4.02}Mn_2Te_4$ and about 14% for $Cu_4Mn_2Te_{3.98}$ in comparison with the un-doped one at 700 K. On the other hand, we remain the Te vacancy while using Cl substitute part Te in $Cu_4Mn_2Te_{3.96-y}Cl_y$ (denoted as **M3**) to further press down the n_H. As shown in Fig. 2f, n_H decreased from 6.9 × 10^{19} cm^{-3} to 4.6 × 10^{19} cm^{-3}, as *y* varied from 0.02 to 0.04, whereas *PF* first increased and then decreased with the decrease of n_H. This suggests that when *y* = 0.03, the hole concentration may be optimized.

The thermal transport properties of $Cu_{4+x}Mn_2Te_{4-\delta-y}Cl_y$ samples in the range of 300–773 K are displayed in Fig. 2d and e. Note that the total thermal conductivity (κ) of $Cu_{4+x}Mn_2Te_{4-\delta-y}Cl_y$ samples is lower than that of pristine $Cu_4Mn_2Te_4$. The turning of the curve of κ in all samples was observed around 730 K, similar turnings are observed in both σ and *S* (Fig. 2a and b). As seen in Fig. 2d, κ exhibits a two staged decrease for these different n_H samples. **M1** and **M2** samples exhibit a staged decrease compared to the pristine sample, while **M3** exhibits another staged decrease. For example, κ decreases from 2.07 W m^{-1} K^{-1} for $Cu_4Mn_2Te_4$ to 1.71 W m^{-1} K^{-1} for $Cu_{4.02}Mn_2Te_4$ and then to 1.13 W m^{-1} K^{-1} for $Cu_4Mn_2Te_{3.92}Cl_{0.04}$ at 700 K. The electronic contribution to the thermal conductivity is calculated using the Wiedemann–Franz relationship $\kappa_e = L\sigma T$, where the Lorenz number *L* can be estimated by fitting experimental Seebeck values in a single parabolic band model.[32] As shown in Fig. S4,† κ_e is very large and decreases with the decrease of n_H. The lattice thermal conductivity (κ_l) is shown in Fig. 2e, in which the electronic term is subtracted from κ. κ_l also exhibits a two staged decrease as κ displays. This indicates that the strategy of **M1–M3** proves to be highly effective for suppressing κ in $Cu_4Mn_2Te_4$-based compounds. The calculated κ_l for the pristine $Cu_4Mn_2Te_4$ sample is 1.16–0.32 W m^{-1} K^{-1}, which is relatively low as we expected. κ_l of **M1** and **M2** samples shows a sudden decrease compared to pristine $Cu_4Mn_2Te_4$. However, there is little difference among these samples. The sudden decrease of κ_l can be ascribed to the phonon scattering by the excess Cu atoms occupying the interstitial site or the formation of vacancies at the Te site. κ_l exhibits another staged decrease in **M3** samples. When the aliovalent Cl is introduced to $Cu_4MnTe_{3.96-y}Cl_y$, the dislocation defect density increases. Combining the phonon scattering by vacancies and dislocation defects, κ_l shows another sudden decrease. Such behaviour is also observed in PbTe[33] and SnTe.[34] This implies that both the interstitial Cu/vacancies of Te and the substitutional impurities of "Cl" can scatter phonons effectively in these samples.

Based on the measured electrical and thermal transport properties, the temperature dependence of the *ZT* value for all samples is calculated and presented in Fig. 3. Due to the increase of *PF* and the reduction of κ, *ZT* was improved in all samples compared to the pristine $Cu_4Mn_2Te_4$. The maximum *ZT* value can reach to 0.4 at 700 K for the $Cu_4Mn_2Te_{3.93}Cl_{0.03}$ sample. Increasing Cl substitution and decreasing n_H do not further increase *ZT*. We wish to stress that the transport data are fully reproducible on temperature cycling to at least 773 K (see the ESI, Fig. S5†).

In summary, a series of spinel-type $Cu_4Mn_2Te_4$-based samples have been successfully prepared and polycrystalline TE properties have been investigated between 300 K and 773 K. Their high TE performances are attributed to the enhanced power factor and low thermal conductivity *via* the

Table 1 Thermoelectric properties of $Cu_{4+x}Mn_2Te_{4-\delta-y}Cl_y$ samples at 300 K and at 700 K

Sample	σ (S cm^{-1})	*S* (μV K^{-1})	*PF* (μW cm^{-1} K^{-2})	κ (W m^{-1} K^{-1})	κ_e (W m^{-1} K^{-1})	κ_l (W m^{-1} K^{-1})	*ZT*
$Cu_4Mn_2Te_4$	1765/1111	27/68	1.3/5.0	2.32/2.13	1.25/1.63	1.09/0.49	0.02/0.17
$Cu_{4.01}Mn_2Te_4$	1618/1000	30/74	1.5/5.4	1.83/1.90	1.13/1.43	0.69/0.48	0.03/0.20
$Cu_{4.02}Mn_2Te_4$	1563/945	33/76	1.7/5.5	1.85/1.70	1.09/1.35	0.77/0.33	0.03/0.22
$Cu_4Mn_2Te_{3.98}$	1537/857	35/82	1.9/5.7	1.76/1.54	1.07/1.19	0.70/0.33	0.03/0.24
$Cu_4Mn_2Te_{3.96}$	1466/797	36/86	1.9/5.8	1.69/1.38	1.02/1.10	0.69/0.27	0.04/0.30
$Cu_4Mn_2Te_{3.94}Cl_{0.02}$	1430/793	38/88	2.1/6.0	1.44/1.23	0.99/1.07	0.47/0.16	0.04/0.34
$Cu_4Mn_2Te_{3.93}Cl_{0.03}$	1407/763	40/90	2.3/6.2	1.48/1.30	0.96/1.05	0.52/0.23	0.05/0.40
$Cu_4Mn_2Te_{3.92}Cl_{0.04}$	1332/694	42/94	2.3/6.0	1.42/1.12	0.91/0.94	0.52/0.20	0.05/0.34

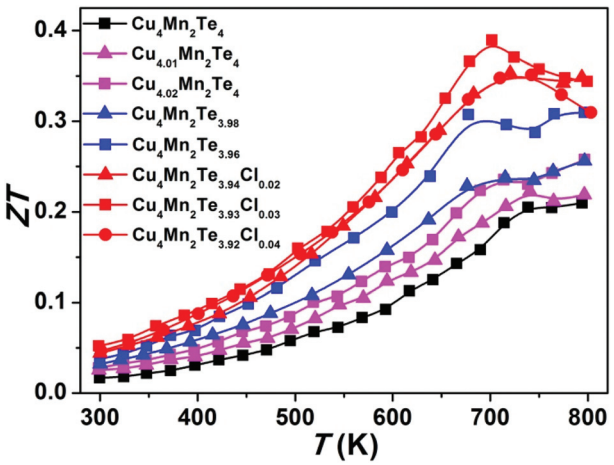

Fig. 3 Temperature dependence of *ZT* values for polycrystalline $Cu_{4+x}Mn_2Te_{4-\delta-y}Cl_y$ samples (x = 0/0.01/0.02, δ = 0, y = 0; x = 0, δ = 0.02/0.04, y = 0; x = 0, δ = 0.04, y = 0.02/0.03/0.04).

synergistic effect of Te-deficiency and Cl-doping. As a result, the peak *ZT* value of 0.4 at 700 K was obtained for the $Cu_4Mn_2Te_{3.93}Cl_{0.03}$ sample, which is two times higher than that of the un-doped polycrystalline $Cu_4Mn_2Te_4$ sample at the same temperature. This work suggests that $Cu_4Mn_2Te_4$-based materials could be promising TE candidates for mid-temperature applications. Further TE performance optimization on this material and the related spinel-type systems is ongoing.

Conflicts of interest

There are no conflicts to declare.

Acknowledgements

This work was supported by the National Natural Science Foundation of China (21771179, 21571020, 21301175, 21233009 and 91422303) and the Natural Science Foundation of Fujian Province (2015J01071).

Notes and references

1 L. E. Bell, *Science*, 2008, **321**, 1457.
2 G. J. Snyder and E. S. Toberer, *Nat. Mater.*, 2008, **7**, 105.
3 J. R. Sootsman, D. Y. Chung and M. G. Kanatzidis, *Angew. Chem., Int. Ed.*, 2009, **48**, 8616.
4 Q. C. Zhang, C. D. Malliakas and M. G. Kanatzidis, *Inorg. Chem.*, 2009, **48**, 10910.
5 K. Biswas, J. Q. He, Q. C. Zhang, G. Y. Wang, C. Uher, V. P. Drvid and M. G. Kanatzidis, *Nat. Chem.*, 2011, **3**, 160.
6 G. J. Tan, L. D. Zhao and M. G. Kanatzidis, *Chem. Rev.*, 2016, **116**, 12123.
7 H. J. Goldsmid, in *CRC Handbook of Thermoelectrics*, ed. D. M. Rowe, CRC Press, Boca Raton, FL, 1995, p. 74.
8 L. D. Zhao, H. J. Wu, S. Q. Hao, C. I. Wu, X. Y. Zhou, K. Biswas, J. Q. He, T. P. Hogan, C. Uher, C. Wolverton, V. P. Dravid and M. G. Kanatzidis, *Energy Environ. Sci.*, 2013, **6**, 3346.
9 Q. Zhang, H. Wang, W. Liu, H. Wang, B. Yu, Q. Zhang, Z. Tian, G. Ni, S. Lee, K. Esfarjani, G. Chen and Z. Ren, *Energy Environ. Sci.*, 2012, **5**, 5246.
10 J. P. Heremans, V. Jovovic, E. S. Toberer, A. Saramat, K. Kurosaki, A. Charoenphakdee, S. Yamanaka and G. J. Snyder, *Science*, 2008, **321**, 554.
11 M. Zebarjadi, G. Joshi, G. H. Zhu, B. Yu, A. Minnich, Y. C. Lan, X. W. Wang, M. Dresselhaus, Z. F. Ren and G. Chen, *Nano Lett.*, 2011, **11**, 2225.
12 J. Martin, L. Wang, L. Chen and G. S. Nolas, *Phys. Rev. B: Condens. Matter Mater. Phys.*, 2009, **79**, 5.
13 W. J. Qiu, L. L. Xi, P. Wei, X. Z. Ke, J. H. Yang and W. Q. Zhang, *Proc. Natl. Acad. Sci. U. S. A.*, 2014, **111**, 15031.
14 H. Lin, H. Chen, J.-S. Yu, Y.-J. Zheng, P.-F. Liu, M. A. Khan and L.-M. Wu, *Dalton Trans.*, 2016, **45**, 11931.
15 M. K. Jana, K. Pal, U. V. Waghmare and K. Biswas, *Angew. Chem., Int. Ed.*, 2016, **55**, 7792.
16 H. Lin, G. J. Tan, J. N. Shen, S. Q. Hao, L. M. Wu, N. Calta, C. Malliakas, S. Wang, C. Wolverton and M. G. Kanatzidis, *Angew. Chem., Int. Ed.*, 2016, **55**, 11431.
17 P. F. Qiu, X. Shi and L. D. Chen, *Energy Storage Mater.*, 2016, **3**, 85.
18 H. Lin, H. Chen, J. N. Shen, L. Chen and L. M. Wu, *Chem. – Eur. J.*, 2014, **20**, 15401.
19 H. Lin, H. Chen, N. Ma, Y.-J. Zheng, J.-N. Shen, J.-S. Yu, X.-T. Wu and L.-M. Wu, *Inorg. Chem. Front.*, 2017, **4**, 1273.
20 H. Liu, X. Shi, F. Xu, L. Zhang, W. Zhang, L. D. Chen, Q. Li, C. Uher, T. Day and G. J. Snyder, *Nat. Mater.*, 2012, **11**, 422.
21 B. Yu, W. S. Liu, S. Chen, H. Wang, H. Z. Wang, G. Chen and Z. F. Ren, *Nano Energy*, 2012, **1**, 472.
22 X. Su, F. Fu, Y. G. Yan, G. Zheng, T. Liang, Q. Zhang, X. Cheng, D. W. Yang, H. Chi, X. F. Tang, Q. J. Zhang and C. Uher, *Nat. Commun.*, 2014, **5**, 4908.
23 L. L. Zhao, X. L. Wang, J. Y. Wang, Z. X. Cheng, S. X. Dou, J. Wang and L. Q. Liu, *Sci. Rep.*, 2014, **5**, 7671.
24 Y. He, T. Day, T. S. Zhang, H. L. Liu, X. Shi, L. D. Chen and G. J. Snyder, *Adv. Mater.*, 2014, **26**, 3974.
25 L. L. Zhao, X. L. Wang, F. Y. Fei, J. Y. Wang, Z. X. Cheng, S. X. Dou, J. Wang and G. J. Snyder, *J. Mater. Chem. A*, 2015, **18**, 9432.
26 Y. He, T. Zhang, X. Shi, S. H. Wei and L. D. Chen, *NPG Asia Mater.*, 2015, **7**, e210.
27 (*a*) X. Lu, D. T. Morelli, Y. Xia, F. Zhou, V. Ozolins, H. Chi, X. Zhou and C. Uher, *Adv. Energy Mater.*, 2012, **3**, 342; (*b*) J. Heo, G. Laurita, S. Muir, M. A. Subramanian and D. A. Keszler, *Chem. Mater.*, 2014, **26**, 2047; (*c*) X. Lu, D. T. Morelli, Y. Xia and V. Ozolins, *Chem. Mater.*, 2015, **27**, 408; (*d*) X. Lu, D. T. Morelli, Y. X. Wang, W. Lai, Y. Xia and V. Ozolins, *Chem. Mater.*, 2016, **28**, 1781.
28 H. Lin, H. Chen, Y.-J. Zheng, Y.-K. Chen, J.-S. Yu and L.-M. Wu, *Chem. Commun.*, 2017, **53**, 2590.

29 H. Chen, H. Lin, Z. X. Lin, J. N. Shen, L. Chen and L.-M. Wu, *Inorg. Chem.*, 2015, **54**, 867.
30 F. K. Lotgering and G. H. A. M. Vandersteen, *J. Phys. Chem. Solids*, 1972, **33**, 2071.
31 L. M. Valiev, I. G. Kerimov and A. A. Abduragimov, *Phys. Status Solidi A*, 1975, **30**, K91.
32 D. P. Spitzer, *J. Phys. Chem. Solids*, 1970, **31**, 19.
33 Z. W. Chen, Z. Z. Jian, W. Li, Y. J. Chang, B. h. Ge, R. Hanus, J. Yang, Y. Chen, M. X. Huang, G. J. Snyder and Y. Z. Pei, *Adv. Mater.*, 2017, **29**, 1606768.
34 Y. Z. Pei, L. L. Zheng, W. Li, S. Q. Lin, Z. W. Chen, Y. Y. Wang, X. F. Xu, H. L. Yu, Y. Chen and B. H. Ge, *Adv. Electron. Mater.*, 2016, **2**, 100019.